


Topological confinement states in ABA trilayer graphene with antiparallel electric fieldJiaqi An^{①,*}, Sanyi You,^{*} Zeyu Li,[†] and Zhenhua Qiao^{②‡}*ICQD, Hefei National Research Center for Physical Sciences at the Microscale,
CAS Key Laboratory of Strongly Coupled Quantum Matter Physics, and Department of Physics,
University of Science and Technology of China, Hefei, Anhui 230026, China* (Received 12 August 2024; revised 3 October 2024; accepted 25 October 2024; published 13 November 2024)

In AB-stacked bilayer graphene, the introduction of an out-of-plane electric field can break the inversion symmetry to open up a nontrivial bulk gap hosting the quantum valley Hall state. However, in ABA-stacked trilayer graphene, the out-of-plane electric field cannot open up a nontrivial valley band gap. By applying a pair of antiparallel electric fields, we theoretically propose three kinds of schemes to open up bulk gaps that harbor the quantum valley Hall effect in the ABA-stacked trilayer graphene. By further considering the small-angle twisted trilayer graphene, we can obtain the topological confinement states along the naturally formed domain walls between ABA- and BAB-stacked regions. It is noteworthy that the synergic effect between the antiparallel electric fields and the magnetic field can open up a nontrivial band gap possessing the quantum valley Hall effect and quantum Hall effect simultaneously. Our work not only theoretically proposes how to realize the quantum valley Hall effect in ABA-trilayer graphene, but also provides an ideal platform to explore the hybrid topological phases.

DOI: [10.1103/PhysRevB.110.L201404](https://doi.org/10.1103/PhysRevB.110.L201404)

Introduction. In condensed matter physics, searching for practical schemes to realize topological quantum materials is always a significant topic [1–6]. At present, it is crucial to increase the observation temperature of various topological states via proper materials design and device manufacturing [7–14]. For different topological systems, such as the \mathbb{Z}_2 topological insulator and quantum anomalous Hall effects, their realization usually needs precise manipulation of spins or spin-orbit couplings, leading to extreme challenges for the experimental realization [15]. Fortunately, another topological state, i.e., the quantum valley Hall effect, can be easily realized by breaking the inversion symmetry of graphene or related two-dimensional systems. For example, introducing staggered sublattice potentials in monolayer graphene, or applying a vertical electric field in AB-stacked bilayer graphene, can open up topologically nontrivial band gaps near valleys K and K' , hosting the quantum valley Hall phases. At the domain walls between different valley Hall topological regions, one-dimensional topological confinement states arise. These states have attracted widespread attention because they rely solely on electrical means, making them a promising alternative for building next-generation high-performance low-power electronic devices [16–43].

With the increasing number of layers, the stacking order of the layers provides a vital degree of freedom to manipulate the properties of two-dimensional materials. For graphene materials, diverse stacking orders make multilayer graphene a fertile ground to realize various quantum states, such as

superconductor and orbital Chern insulator [44–50]. In the case of trilayer graphene, the ABA and ABC stacking are two typical stable stacking configurations, respectively. The ABA-stacked trilayer graphene has captured broad interest due to its unique properties of coexisting linear Dirac dispersion and parabolic dispersion relations [51–62]. Unfortunately, the ABA-stacked trilayer graphene cannot open a nontrivial energy gap only through an out-of-plane electric field as simple as the ABC-stacked one to realize the quantum valley Hall effect [28]. Therefore, it is still challenging to open up a topological valley band gap in ABA trilayer graphene.

In this work, we theoretically show that, by introducing a pair of antiparallel electric fields [63] in ABA-stacked trilayer graphene, a nontrivial quantum valley Hall gap is opened, accompanying a Dirac cone pinned on one of the nontrivial bands. To remove the influence of bulk states contributed by the Dirac cone, three schemes are proposed to open up the global gap in the system, thereby realizing the quantum valley Hall states. Based on the previous discussion of the topological confinement states, we need a domain wall separating different valley Hall topological regions. Fortunately, we obtain natural ABA/BAB-stacked domain walls to realize the topological confinement states in the minimally twisted trilayer graphene systems with the same twisting angles for the first time. Our work provides an experimentally friendly proposal for the realization of the topological confinement states in minimally twisted trilayer graphene. Moreover, the combination of an antiparallel electric field and a magnetic field can realize the hybrid topological states, i.e., the coexisting quantum valley Hall effect and quantum Hall effect simultaneously [64]. Our findings strongly indicate that ABA-stacked trilayer graphene is a superior platform for investigating novel quantum effects and for building high-performance quantum devices.

*These authors contributed equally to this work.

†Contact author: lzy92@ustc.edu.cn

‡Contact author: qiao@ustc.edu.cn

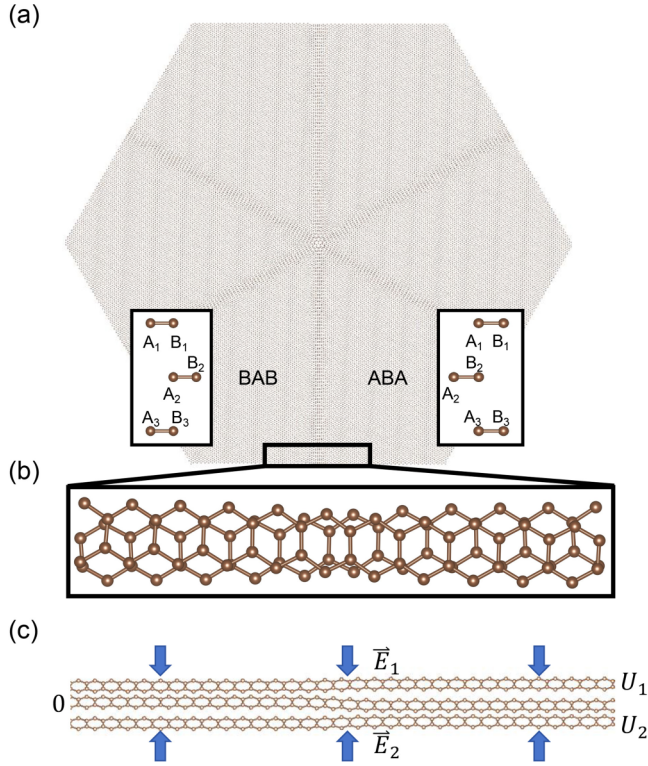


FIG. 1. (a) Twisted trilayer graphene with ABA-stacked region (A_1, B_2, A_3 atoms are on top of each other) and BAB-stacked region (B_1, A_2, B_3 atoms are on top of each other). In the ABA-stacked region, we assign specific labels to the atoms as $A_1, B_1, A_2, B_2, A_3,$ and B_3 . (b) Zoomed-in view of the stacked area near the domain wall. (c) Side view of ribbon cell exhibiting the antiparallel fields.

Structural analysis. As mentioned above, we mainly focus on the twisted trilayer graphene, which harbors the natural ABA/BAB-stacked domain wall. We adopt the same method in Refs. [65,66] to design a commensurate cell for trilayer graphene. Six indices are needed to determine a commensurate cell of the twisted trilayer graphene. However, only four indices are necessary in this work because the top and bottom layers are completely aligned. We choose the middle layer as the reference layer. The lattice vectors for the middle layer can be represented as \mathbf{a}_1 and \mathbf{a}_2 , respectively. The two lattice vectors of the commensurate supercell \mathbf{r}_1 and \mathbf{r}_2 can be expressed as

$$\begin{pmatrix} \mathbf{r}_1 \\ \mathbf{r}_2 \end{pmatrix} = \mathbf{M}' \cdot \begin{pmatrix} \mathbf{a}_1 \\ \mathbf{a}_2 \end{pmatrix}, \quad (1)$$

where we use the transformation matrices

$$\mathbf{M} = \begin{pmatrix} p & q \\ -q & p+q \end{pmatrix}, \quad \mathbf{M}' = \begin{pmatrix} p' & q' \\ -q' & p'+q' \end{pmatrix}. \quad (2)$$

The top and bottom layer lattice vectors $\mathbf{a}'_1, \mathbf{a}'_2$ can also be related via

$$\begin{pmatrix} \mathbf{a}'_1 \\ \mathbf{a}'_2 \end{pmatrix} = \mathbf{M}'^{-1} \cdot \mathbf{M} \cdot \begin{pmatrix} \mathbf{a}_1 \\ \mathbf{a}_2 \end{pmatrix}, \quad (3)$$

and the rotation angle θ between top and middle layer (or bottom to middle layer) is

$$\cos(\theta) = \frac{1}{2\alpha g} [2p'p + 2q'q + p'q + q'p], \quad (4)$$

where $g = m^2 + n^2 + mn$.

As displayed in Fig. 1(a), we build a sandwiched twisted trilayer graphene after relaxation. The indices to build the moiré cell are $p = 251, q = 250, p' = 250, q' = 251$, and the rotation angle is $\theta = 0.13^\circ$. We could tailor the ribbon structure as displayed in Fig. 1(b), where the domain wall between ABA- and BAB-stacked regions emerges. Figure 1(b) is considered as the ribbon cell with a domain wall structure, i.e., all the following ribbon band-structure calculations are based on Fig. 1(b).

To study the relaxation effects in twisted trilayer graphene, we perform energy minimization by using the large-scale atomic/molecular massively parallel simulator (LAMMPS) package [67,68]. For the interlayer interactions, we employ the dihedral-angle-corrected registry-dependent interlayer (DRIP) potential that has been reparametrized [69] using the exact-exchange-random phase approximation (EXX-RPA) density functional theory (DFT) calculations [70], which includes dihedral angle corrections based on the well-known registry-dependent Kolmogorov-Crespi (KC) potential [71]. We use the reactive empirical bond-order 2 (REBO2) potential to simulate the intralayer interactions. [72].

Tight-binding Hamiltonian of twisted trilayer graphene. Based on the Slater-Koster method, a tight-binding Hamiltonian model [Eq. (8)] is constructed to precisely capture the electronic properties of the ribbon structure with the domain wall from the relaxed twisted trilayer graphene [Fig. 1(b)]. The hopping terms for both interlayer and intralayer couplings have the same expression as [73–75]

$$t_{ij} = V_{pp\pi}(\mathbf{r}_{ij}) \left[1 - \left(\frac{\mathbf{r}_{ij} \cdot \mathbf{e}_z}{|\mathbf{r}_{ij}|} \right)^2 \right] + V_{pp\sigma}(\mathbf{r}_{ij}) \left(\frac{\mathbf{r}_{ij} \cdot \mathbf{e}_z}{|\mathbf{r}_{ij}|} \right)^2, \quad (5)$$

with

$$V_{pp\pi}(\mathbf{r}_{ij}) = V_{pp\pi}^0 \exp\left(-\frac{|\mathbf{r}_{ij}| - a_{CC}}{r_0}\right), \quad (6)$$

and

$$V_{pp\sigma}(\mathbf{r}_{ij}) = V_{pp\sigma}^0 \exp\left(-\frac{|\mathbf{r}_{ij}| - c_0}{r_0}\right), \quad (7)$$

where \mathbf{r}_{ij} represents the distance vector between i th and j th atoms, and $\mathbf{r}_{ij} \cdot \mathbf{e}_z$ represents the interlayer distance between the i th and j th atoms. The other parameters are set to be $V_{pp\pi}^0 = -2.7$ eV, $V_{pp\sigma}^0 = 0.48$ eV, $a_{CC} = a_G/\sqrt{3} = 1.42$ Å, $c_0 = 3.35$ Å, and $r_0 = 0.184a_G$, where a_G is the lattice constant of graphene.

The main Hamiltonian can be written as

$$H = \sum_{ij} t_{ij} c_i^\dagger c_j + \sum_{i \in \text{Top}} U_1 c_i^\dagger c_i + \sum_{i \in \text{Middle}} U_2 c_i^\dagger c_i + \sum_{i \in \text{Bottom}} U_3 c_i^\dagger c_i, \quad (8)$$

where U_1 , U_2 , and U_3 are the onsite energies for each layer in twisted trilayer graphene, respectively. One can set $U_1 = U_3 = U$ to generate the antiparallel electric field. Simply but without loss of generality, we always set $U_2 = 0$ eV. Although the antiparallel electric field can open up a gap harboring the quantum valley Hall effect, there is still a Dirac dispersion remaining within the gap. Here, we propose three approaches to manipulate the system to open up a global band gap.

The first approach is to apply different electric potentials at each layer, i.e., $U_1 \neq U_3$. The second approach is to add a small δ on different sublattices, with the Hamiltonian being modified as

$$H = \sum_{ij} -t_{ij}c_i^\dagger c_j + \sum_{i \in \text{Top}} (U_1 \pm \delta)c_i^\dagger c_i + \sum_{i \in \text{Middle}} U_2 c_i^\dagger c_i + \sum_{i \in \text{Bottom}} (U_3 \pm \delta)c_i^\dagger c_i. \quad (9)$$

Here, setting $U_1 = U_3 = U$, $U_2 = 0$, we choose $+\delta$ for the A sublattice (atoms A_1 and A_3 in Fig. 1) and $-\delta$ for the B sublattice (atoms B_1 and B_3 in Fig. 1) in the ABA region. The signs of δ for A and B sublattices are reversed in the BAB region. The third approach is to apply a magnetic field [26] to generate the Landau level, which shifts the bulk state of the Dirac cone from the global gap but the topological confinement states are unaffected. In the presence of a perpendicular magnetic field $B = \nabla \times \vec{A}$, the tight-binding Hamiltonian [Eq. (8)] can be modified by introducing the Peierls term in the hopping terms, i.e., t_{ij} becomes $t_{ij}e^{ie/\hbar \int A \cdot dl}$.

Low-energy continuum model of ABA-stacked trilayer graphene. To effectively figure out the bulk electronic and topological properties, we construct a six-band effective model for the trilayer ABA-stacked graphene. On the basis of $\{\psi_{A_1}, \psi_{B_1}, \psi_{A_2}, \psi_{B_2}, \psi_{A_3}, \psi_{B_3}\}$, the Hamiltonian is expressed as

$$H = \begin{pmatrix} U_1 & \frac{3}{2}at\tau_{xy} & & & & -\gamma \\ \frac{3}{2}at\tau_{xy}^* & U_1 & & & & \\ & & U_2 & \frac{3}{2}at\tau_{xy} & & \\ -\gamma & & \frac{3}{2}at\tau_{xy}^* & U_2 & & -\gamma \\ & & & -\gamma & U_3 & \frac{3}{2}at\tau_{xy} \\ & & & & \frac{3}{2}at\tau_{xy}^* & U_3 \end{pmatrix}, \quad (10)$$

where $t = -2.7$ eV represents the energy of intralayer nearest-neighbor hopping, while $a = 2.46$ Å denotes the lattice constant. We introduce $\tau_{xy} = v_x + iv_y$ to represent the momentum near valley K . $\gamma = 0.48$ eV is the hopping energy between carbon atoms at the top site in ABA-stacked trilayer graphene, i.e., between A_1 and B_2 , as well as between B_2 and A_3 .

Based on this effective Hamiltonian, one can calculate the valley Chern number. The Berry connection can be expressed as [76]

$$b(k) = \nabla \times a(k), \quad (11)$$

and the corresponding Berry phase is

$$\Phi = \oint d^2kz \cdot b(k). \quad (12)$$

By using the Wilson loop method, Φ_n can be expressed as

$$\Phi_n = \text{Arg} \left[\prod_p \text{Det}[\langle u_s(k_{n,p}) | u'_s(k_{n,p+1}) \rangle] \right], \quad (13)$$

where s labels the band index. The valley Chern number is

$$C_v = 1/2\pi \sum \Phi_n. \quad (14)$$

By using this formalism, the valley Chern number can be calculated even for the system with band overlapped.

Antiparallel electric field in ABA/BAB-stacked trilayer graphene. Using the six-band effective model of ABA trilayer graphene, we first calculate the band structure near valley K without external fields, i.e., $U_1 = U_2 = U_3 = 0$, as shown in Fig. 2(a). The band structure consists of Dirac and parabolic dispersion relations, a quadruple degenerate point appearing at $E_f = 0$ eV. Figure 2(b) displays the ribbon band structure [see Fig. 1(b)]. When the antiparallel electric field is introduced, i.e., $U_1 = U_3 = 0.1$ eV, $U_2 = 0$ eV. The corresponding bulk band structures around valley K are displayed in Fig. 2(c), with bands being sequentially labeled from bottom to top as 1 to 6. Interestingly, this antiparallel electric field opens an energy gap about 0.1 eV between bands 3 and 4. To our surprise, the obtained valley Chern number indicates that it is topologically nontrivial with $C_v = 1$. Additionally, one can see that the linearly dispersed Dirac bands [see Fig. 2(c)] shift upward by a value, being the same as the energy gap between bands 3 and 4. This leads to the pinning of the Dirac cone at band 4, forming a triply degenerate point. Correspondingly, the energy bands of the ribbon system are displayed in Fig. 2(d), where two pairs of topological confinement states with opposite group velocities are submerged in the bulk states belonging to the Dirac dispersion. The number of topological confinement states is determined by the difference of valley Chern numbers of the regions separated by the domain wall, obeying the bulk-boundary correspondence. Moreover, it is noteworthy that the sizes of the bulk energy gap and the nontrivial energy gap of the strip also essentially coincide.

Furthermore, as displayed in Figs. 2(e1)–2(e6), we calculate the modulus squared of the wave function near valley K for the six bands in Fig. 2(c). For bands 1, 6 and bands 3, 4, the corresponding the modulus squared of wave function is distributed at all layers. In the top and bottom layers, the curves are degenerate. With the variation of the wave vector, the curves of the bottom/top layer show opposite trends compared with that of the middle layer. For bands 2 and 5, the modulus squared of wave function is only equally distributed at the top and bottom layers. This indicates that the wave-function distributions of the Dirac dispersion are only at the outer layers (top and bottom layers). Therefore, we pose a reasonable question. Our goal is to open up a global energy gap in this system to find topological confinement states induced by valley topological difference. Now that it has been established that the bulk states contributed by the Dirac cones are entirely distributed in the system's outer layers, can we only manipulate the system's outermost layers to open up a gap at this Dirac cone while preserving the quantum valley Hall phase introduced by the antiparallel electric field? Following this line of thought, we undertake attempts below.

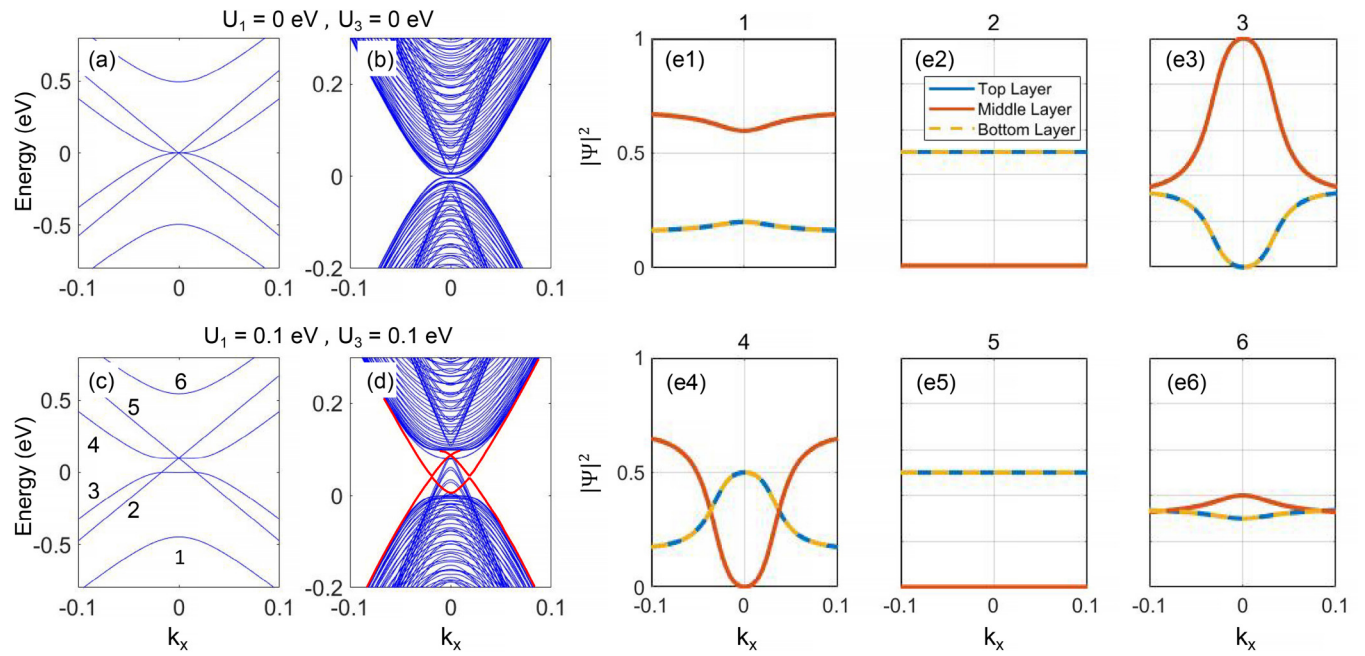


FIG. 2. (a), (b) Band structures of the bulk and ribbon for the ABA-stacked trilayer graphene. (c), (d) Band structures of the bulk and ribbon after applying the antiparallel electric field, i.e., $U_1 = U_3 = 0.1$ eV, $U_2 = 0$ eV. Red lines in (d) are the topological confinement states. (e1)–(e6) The modulus squared of wave function of the six energy bands labeled in (c).

Valley Chern number phase diagram. In the following cases, i.e., $U_1 \neq U_3$, the system enters different phases. Here, we present the phase diagram of valley Chern number in the (U_1, U_3) plane, as displayed in Fig. 3(a). One can notice that the valley Chern number varies between -1 to 1 .

Along the green line in the phase diagram at fixed $U_1 = 0.1$ [see Fig. 3(a)], we calculate the bulk band structures around valley K at the specific positions, as displayed in Figs. 3(b1)–3(b5). By tuning the value of U_3 from 0.2 to -0.2 , one can see that the global band gap can be opened when $U_3 = 0.2, 0.0$, and -0.2 . Correspondingly, the valley Chern number $C_v = 0.5, 0.5$, and -0.5 . When $U_1 = 0.1 = -U_3$, i.e., under

a uniform perpendicular electric field, the system goes into a normal metal phase with $C_v = 0$, as displayed in Fig. 3(b4). Interestingly, when $U_1 = 0.1$ and $U_3 = 0.2$, it is noticed that all the intersections of the Dirac cone and other bands open energy gaps due to the topological phase transition. We also calculate the ribbon band structures based on the relaxed ABA/BAB domain wall. The topological confinement states can be observed in Figs. 3(c1), 3(c3), and 3(c5), respectively. The number of topological confinement states is determined by the difference of valley Chern number.

Let us now move to the second approach. Besides the antiparallel electric field, i.e., $U_1 = U_3 = U$ and $U_2 = 0$, we

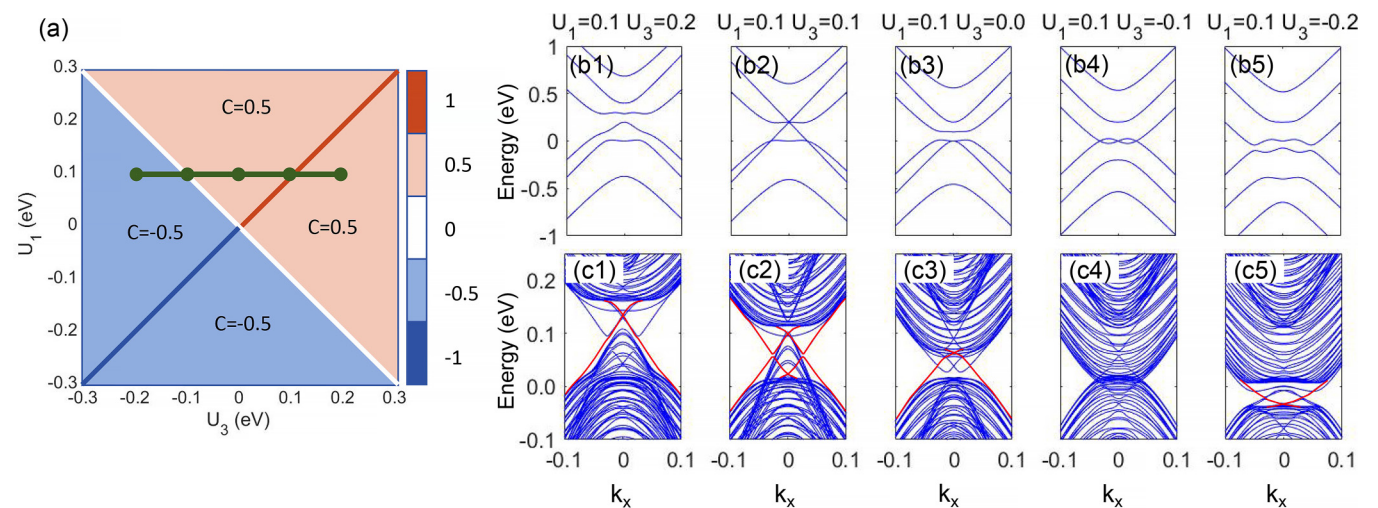


FIG. 3. (a) Phase diagram of valley Chern number at the plane of U_1 and U_3 . (b1)–(b5) Bulk band structures following the deep green line in (a). (c1)–(c5) Corresponding ribbon band structures. The ribbon structure is the same as that in Fig. 1(d). Red lines in (c) are the topological confinement states.

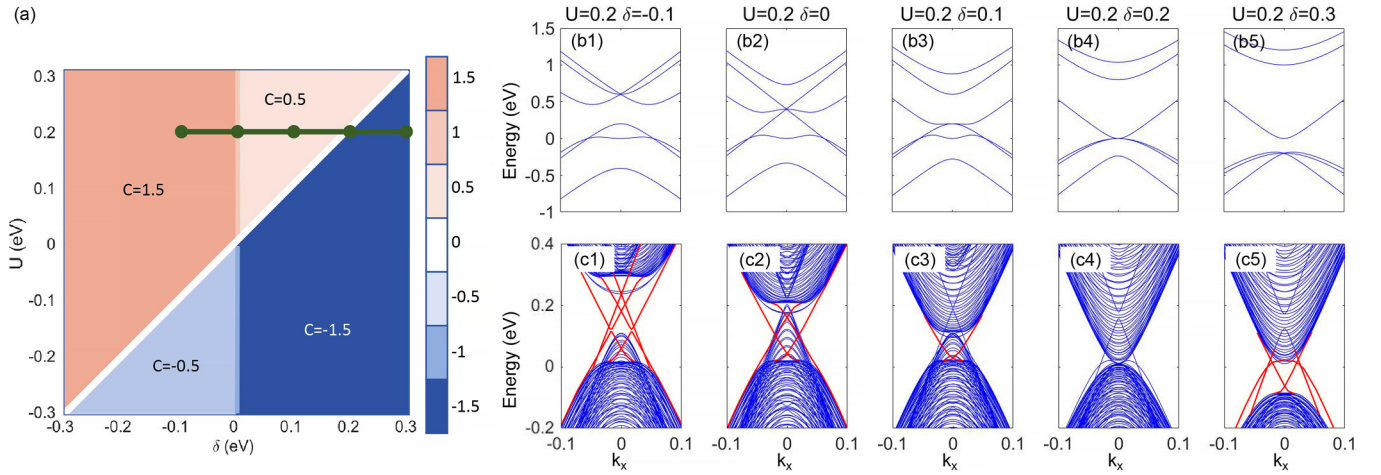


FIG. 4. (a) Phase diagram of valley Chern number in the plane of U and δ . (b1)–(b5) Bulk band structures following the deep green line in (a). (c1)–(c5) Corresponding ribbon band structures. The ribbon structure is the same as Fig. 1(d). Red lines in (c) are the topological confinement states.

further add a small staggered sublattice potential $\pm\delta$ on the top and bottom layers, respectively. Theoretically, this staggered sublattice potential can open up a nontrivial energy gap in the system characterized by the Dirac dispersion. Here, we set U and δ in the range between -0.3 and 0.3 eV to obtain a phase diagram of the valley Chern number, as displayed in Fig. 4(a), where the valley Chern number can be switched from -1.5 to 1.5 . Similarly, along the green line in the phase diagram with fixed $U = 0.2$ [see Fig. 4(a)], we calculate the bulk band structures around valley K at the specific positions, as shown in Figs. 4(b1)–4(b5). By tuning the value of δ from -0.1 to 0.3 , one can see the global band gap can be opened, when $\delta = -0.1$ and $\delta = 0.3$ [see Figs. 4(b1) and 4(b5)]. Correspondingly, the valley Chern number $C_v = 1.5$ and $C_v = -1.5$. When $\delta = 0.0$, the system returns to the situation where

$U_1 = U_3$. When $\delta = 0.1$ or $\delta = 0.2$, the system is still in a metallic phase. Besides the bulk band structures, we also calculate the corresponding ribbon band structures, as displayed in Figs. 4(c1)–4(c5). The topological confinement states can be observed clearly in Figs. 4(c1) and 4(c5), where the number of topological confinement states is equal to the difference of the valley Chern number. It is noteworthy that, as displayed in Figs. 4(b1) and 4(c1), one of the topological confinement states possesses the feature of monolayer graphene, which implies the existence of hybrid topological states consisting of monolayer and bilayer topological confinement states. Furthermore, our ribbon is formed by the relaxed ABA/BAB domain wall, where the stacking order of carbon atoms can be changed. To realize topological confinement states, it is necessary to reverse the sign of δ after passing through the domain

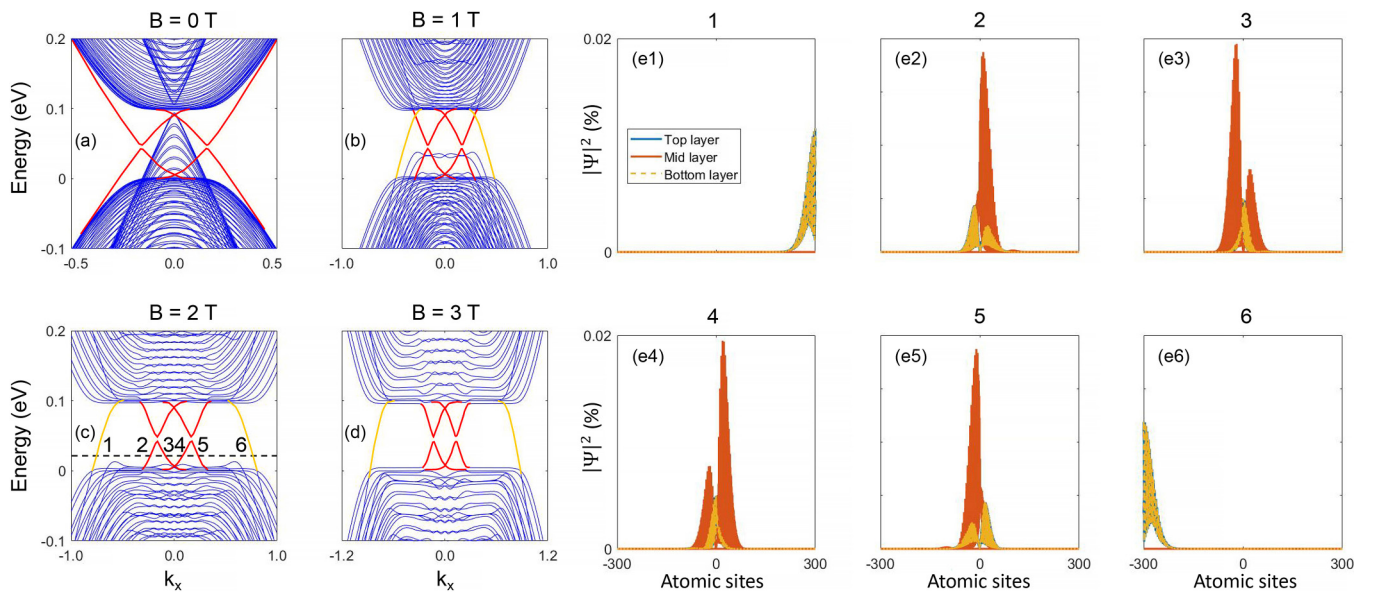


FIG. 5. (a)–(d) Ribbon band structure with the antiparallel electric field and magnetic field. Red lines are the topological confinement states and yellow lines are the quantum Hall edge states. The parameters are chosen to be $U_1 = U_3 = 0.1$ eV, $U_2 = 0$ eV. (e1)–(e6) The modulus squared of wave function in (c), labeled from 1 to 6 at $E_f = 0.02$ eV.

wall. This operation also offers a plausible explanation for the appearance of the topological confinement state contributed by monolayer graphene.

The influence of magnetic field. In condensed matter physics, applying a magnetic field is a common research technique. We then demonstrate that the cooperation of an antiparallel electric field and a perpendicular magnetic field can effectively open up a topologically nontrivial global gap in the trilayer graphene system. For convenience and in contrast to the two approaches mentioned above, we add the magnetic field in all three layers. For similarity, we set $U_1 = U_3 = -0.05$ eV. When the magnetic field is absent, i.e., $B = 0$ T, the system is a metal with a Dirac cone as previously mentioned. With the increase of the magnetic field, the bulk states contributed to by the Dirac cone are gradually suppressed. Then, two pairs of topological confinement states with opposite group velocities emerge. When the magnetic field reaches 3 T, the Dirac cone transforms into discrete Landau levels falling in the gap of the quantum valley Hall, as displayed in Fig. 5(d). In this gap, two pairs of topological confinement states and a pair of quantum Hall edge states with opposite group velocities can be observed clearly, which implies that the hybrid topological states can coexist in this system. Furthermore, our previous work demonstrated that a magnetic field can significantly enhance the robustness of topological confinement states [26]. Thus, it is promising to simultaneously observe both the quantum valley Hall and quantum Hall effects in this system. For clarity, we explore the situation with $B = 2$ T and choose different positions corresponding to topological confinement states or quantum Hall edge states marked by numbers 1 to 6 in Fig. 5(c). It is evident that the localized topological confinement states, respectively, numbers 2, 3,

4, and 5, are distributed along the domain walls throughout three layers, as displayed in Figs. 5(e2)–5(e5). Meanwhile, the quantum Hall edge states 1 and 6 are equally distributed at the top and bottom layers along the left and right boundaries [see Figs. 5(e1) and 5(e6)], respectively.

Conclusion. In this study, by introducing a pair of identical antiparallel electric fields, we successfully open up a gap harboring the quantum valley Hall effect in ABA-stacked trilayer graphene for the first time. Meanwhile, there is a Dirac cone pinned on the conduction band nearest to the Fermi level. Three methods are used to open up a global energy gap where the quantum valley Hall effect is preserved. Then, based on small-angle twisted trilayer graphene, we obtain topological confinement states along the domain wall between ABA/BAB stacking regions. Particularly, one of the methods combining the antiparallel electric fields and the magnetic field provides a platform to explore the quantum valley Hall effect and quantum Hall effect at the same time. Our work paves the way for exploring novel topological quantum states and designing low-power quantum devices.

Acknowledgments. We acknowledge the financial support from the National Natural Science Foundation of China (Grants No. 11974327 and No. 12004369), Anhui Initiative in Quantum Information Technologies (Grant No. AHY170000), the Innovation Program for Quantum Science and Technology (Grant No. 2021ZD0302800), and China Postdoctoral Science Foundation (Grants No. 2023M733411 and No. 2023TQ0347). We also thank the Supercomputing Center of University of Science and Technology of China for providing the high-performance computing resources.

-
- [1] L. Fu, C. L. Kane, and E. J. Mele, Topological insulators in three dimensions, *Phys. Rev. Lett.* **98**, 106803 (2007).
- [2] M. Z. Hasan and C. L. Kane, *Colloquium: Topological insulators*, *Rev. Mod. Phys.* **82**, 3045 (2010).
- [3] X. L. Qi and S. C. Zhang, Topological insulators and superconductors, *Rev. Mod. Phys.* **83**, 1057 (2011).
- [4] O. Breunig and Y. Ando, Opportunities in topological insulator devices, *Nat. Rev. Phys.* **4**, 184 (2022).
- [5] F. Liu, Two-dimensional topological insulators: past, present and future, *Coshare Sci.* **01**, 03 (2023).
- [6] Y. Tokura, K. Yasuda, and A. Tsukazaki, Magnetic topological insulators, *Nat. Rev. Phys.* **1**, 126 (2019).
- [7] Z. Qiao, S. A. Yang, W. Feng, W. K. Tse, J. Ding, Y. Yao, J. Wang, and Q. Niu, Quantum anomalous Hall effect in graphene from Rashba and exchange effects, *Phys. Rev. B* **82**, 161414(R) (2010).
- [8] Z. Wang, C. Tang, R. Sachs, Y. Barlas, and J. Shi, Proximity-induced ferromagnetism in graphene revealed by the anomalous Hall effect, *Phys. Rev. Lett.* **114**, 016603 (2015).
- [9] C. Z. Chang, J. Zhang, X. Feng, J. Shen, Z. Zhang, M. Guo, K. Li, Y. Ou, P. Wei, L. L. Wang, Z. Q. Ji, Y. Feng, S. Ji, X. Chen, J. Jia, X. Dai, Z. Fang, S. C. Zhang, K. He, Y. Wang *et al.*, Experimental observation of the quantum anomalous Hall effect in a magnetic topological insulator, *Science* **340**, 167 (2013).
- [10] Y. Deng, Y. Yu, M. Z. Shi, Z. Guo, Z. Xu, J. Wang, X. H. Chen, and Y. Zhang, Quantum anomalous Hall effect in intrinsic magnetic topological insulator, *Science* **367**, 895 (2020).
- [11] S. Qi, Z. Qiao, X. Deng, E. D. Cubuk, H. Chen, W. Zhu, E. Kaxiras, S. B. Zhang, X. Xu, and Z. Zhang, High-temperature quantum anomalous Hall effect in n - p codoped topological insulators, *Phys. Rev. Lett.* **117**, 056804 (2016).
- [12] B. A. Bernevig, T. L. Hughes, and S. C. Zhang, Quantum spin Hall effect and topological phase transition in HgTe quantum wells, *Science* **314**, 1757 (2006).
- [13] M. Liu, J. Zhang, C. Z. Chang, Z. Zhang, X. Feng, K. Li, K. He, L. L. Wang, X. Chen, X. Dai, Z. Fang, Q. K. Xue, X. Ma, and Y. Wang, Crossover between weak antilocalization and weak localization in a magnetically doped topological insulator, *Phys. Rev. Lett.* **108**, 036805 (2012).
- [14] H. Pan, Z. Li, C. C. Liu, G. Zhu, Z. Qiao, and Y. Yao, Valley-polarized quantum anomalous Hall effect in silicene, *Phys. Rev. Lett.* **112**, 106802 (2014).

- [15] C. Z. Chang, C. X. Liu, and A. H. Macdonald, *Colloquium: Quantum anomalous Hall effect*, *Rev. Mod. Phys.* **95**, 011002 (2023).
- [16] I. Martin, Y. M. Blanter, and A. F. Morpurgo, Topological confinement in bilayer graphene, *Phys. Rev. Lett.* **100**, 036804 (2008).
- [17] J. Li, K. Wang, K. J. McFaul, Z. Zern, Y. Ren, K. Watanabe, T. Taniguchi, Z. Qiao, and J. Zhu, Gate-controlled topological conducting channels in bilayer graphene, *Nat. Nanotechnol.* **11**, 1060 (2016).
- [18] J. Li, R. X. Zhang, Z. Yin, J. Zhang, K. Watanabe, T. Taniguchi, C. Liu, and J. Zhu, A valley valve and electron beam splitter, *Science* **362**, 1149 (2018).
- [19] G. W. Semenoff, V. Semenoff, and F. Zhou, Domain walls in gapped graphene, *Phys. Rev. Lett.* **101**, 087204 (2008).
- [20] Z. Yan, T. Hou, Y. Han, X. Xu, and Z. Qiao, Electronic properties of zero-line modes in bilayer graphene: An *ab initio* study, *Phys. Rev. B* **105**, 035425 (2022).
- [21] Z. Qiao, J. Jung, Q. Niu, and A. H. MacDonald, Electronic highways in bilayer graphene, *Nano Lett.* **11**, 3453 (2011).
- [22] Z. Qiao, J. Jung, C. Lin, Y. Ren, A. H. MacDonald, and Q. Niu, Current partition at topological channel intersections, *Phys. Rev. Lett.* **112**, 206601 (2014).
- [23] T. Hou, G. Cheng, W.-K. Tse, C. Zeng, and Z. Qiao, Topological zero-line modes in folded bilayer graphene, *Phys. Rev. B* **98**, 245417 (2018).
- [24] X. Bi, J. Jung and Z. Qiao, Role of geometry and topological defects in the one-dimensional zero-line modes of graphene, *Phys. Rev. B* **92**, 235421 (2015).
- [25] L. Ju, Z. Shi, N. Nair, Y. Lv, C. Jin, J. Velasco Jr., C. Ojeda-Aristizabal, H. A. Bechtel, M. C. Martin, A. Zettl, J. Analytis, and F. Wang, Topological valley transport at bilayer graphene domain walls, *Nature (London)* **520**, 650 (2015).
- [26] K. Wang, T. Hou, Y. Ren, and Z. Qiao, Enhanced robustness of zero-line modes in graphene via magnetic field, *Front. Phys.* **14**, 23501 (2019).
- [27] W. Yao, S. A. Yang, and Q. Niu, Edge states in graphene: From gapped flat-band to gapless chiral modes, *Phys. Rev. Lett.* **102**, 096801 (2009).
- [28] J. Jung, F. Zhang, Z. Qiao, and A. H. MacDonald, Valley-Hall kink and edge states in multilayer graphene, *Phys. Rev. B* **84**, 075418 (2011).
- [29] H. Pan, X. Li, F. Zhang, and S. A. Yang, Perfect valley filter in a topological domain wall, *Phys. Rev. B* **92**, 041404(R) (2015).
- [30] C. Lee, G. Kim, J. Jung, and H. Min, Zero-line modes at stacking faulted domain walls in multilayer graphene, *Phys. Rev. B* **94**, 125438 (2016).
- [31] M. Kim, J. H. Choi, S. H. Lee, K. Watanabe, T. Taniguchi, S. H. Jhi, and H. J. Lee, Valley-symmetry-preserved transport in ballistic graphene with gate-defined carrier guiding, *Nat. Phys.* **12**, 1022 (2016).
- [32] S. G. Cheng, H. Liu, H. Jiang, Q. F. Sun, and X. C. Xie, Manipulation and characterization of the valley-polarized topological kink states in graphene-based interferometers, *Phys. Rev. Lett.* **121**, 156801 (2018).
- [33] J. R. Anglin and A. Schulz, Analytical solutions of the two-dimensional Dirac equation for a topological channel intersection, *Phys. Rev. B* **95**, 045430 (2017).
- [34] K. Wang, Y. Ren, X. Deng, S. A. Yang, J. Jung, and Z. Qiao, Gate-tunable current partition in graphene-based topological zero lines, *Phys. Rev. B* **95**, 245420 (2017).
- [35] Y. Ren, J. Zeng, K. Wang, F. Xu, and Z. Qiao, Tunable current partition at zero-line intersection of quantum anomalous Hall topologies, *Phys. Rev. B* **96**, 155445 (2017).
- [36] Y. T. Zhang, Z. Qiao, and Q. F. Sun, Detecting zero-line mode in bilayer graphene via the quantum Hall effect, *Phys. Rev. B* **87**, 235405 (2013).
- [37] M. Wang, L. Liu, C. C. Liu, and Y. Yao, van der Waals heterostructures of germanene, stanene, and silicene with hexagonal boron nitride and their topological domain walls, *Phys. Rev. B* **93**, 155412 (2016).
- [38] F. Zhang, A. H. MacDonald, and E. J. Mele, Valley Chern numbers and boundary modes in gapped bilayer graphene, *Proc. Natl. Acad. Sci. USA* **110**, 10546 (2013).
- [39] Y. Han, S. You, and Z. Qiao, Interchannel coupling induced gapless modes in multichannel zero-line systems, *Phys. Rev. B* **105**, 155301 (2022).
- [40] M. Yankowitz, J. I. J. Wang, A. G. Birdwell, Y. Chen, K. Watanabe, T. Taniguchi, P. Jacquod, P. San-Jose, P. Jarillo-Herrero, and B. J. LeRoy, Electric field control of soliton motion and stacking in trilayer graphene, *Nat. Mater.* **13**, 786 (2014).
- [41] J. Zeng, R. Xue, T. Hou, Y. Han, and Z. Qiao, Formation of topological domain walls and quantum transport properties of zero-line modes in commensurate bilayer graphene systems, *Front. Phys.* **17**, 63503 (2022).
- [42] A. O. Fumega and J. L. Lado, Ferroelectric valley valves with graphene/MoTe₂ van der Waals heterostructures, *Nanoscale* **15**, 2181 (2023).
- [43] V. V. Enaldiev, C. Moulds, A. K. Geim, V. I. Fal'ko, Non-chiral one-dimensional sates propagating inside AB/BA domain walls in bilayer graphene, *Academia Nano: Science, Materials, Technology* **1**, 1 (2024).
- [44] H. Zhou, T. Xie, T. Taniguchi, K. Watanabe, and A. F. Young, Superconductivity in rhombohedral trilayer graphene, *Nature (London)* **598**, 434 (2021).
- [45] T. Han, Z. Lu, G. Scuri, J. Sung, J. Wang, T. Han, K. Watanabe, T. Taniguchi, H. Park, and L. Ju, Correlated insulator and Chern insulators in pentalayer rhombohedral-stacked graphene, *Nat. Nanotechnol.* **19**, 181 (2024).
- [46] L. Yang, S. Ding, J. Gao, and M. Wu, Atypical sliding and moiré ferroelectricity in pure multilayer graphene, *Phys. Rev. Lett.* **131**, 096801 (2023).
- [47] A. Garcia-Ruiz, V. Enaldiev, A. McEllistrim, and V. I. Fal'ko, Mixed-stacking few-layer graphene as an elemental weak ferroelectric material, *Nano Lett.* **23**, 4120 (2023).
- [48] T. Han, Z. Lu, G. Scuri, J. Wang, T. Han, K. Watanabe, T. Taniguchi, L. Fu, H. Park, and L. Ju, Orbital multiferoicity in pentalayer rhombohedral graphene, *Nature (London)* **623**, 41 (2023).
- [49] S. You, T. Hou, Z. Li, and Z. Qiao, Physical origin of current partition at a topological trifurcation, *Phys. Rev. B* **106**, L161413 (2022).
- [50] S. You, J. An, and Z. Qiao, Spin resolved zero-line modes in minimally twisted bilayer graphene from exchange field and gate voltage, *Chinese Physics Letters* **41**, 077301 (2024).

- [51] S. K. Srivastav, A. Udupa, K. Watanabe, T. Taniguchi, D. Sen, and A. Das, Electric-field-tunable edge transport in bernal-stacked trilayer graphene, *Phys. Rev. Lett.* **132**, 096301 (2024).
- [52] E. A. Henriksen, D. Nandi, and J. P. Eisenstein, Quantum Hall effect and semimetallic behavior of dual-gated ABA-stacked trilayer graphene, *Phys. Rev. X* **2**, 011004 (2012).
- [53] C. Cong, T. Yu, K. Sato, J. Shang, R. Saito, G. F. Dresselhaus, and M. S. Dresselhaus, Raman characterization of ABA- and ABC-stacked trilayer graphene, *ACS Nano* **5**, 8760 (2011).
- [54] M. Koshino and E. McCann, Gate-induced interlayer asymmetry in ABA-stacked trilayer graphene, *Phys. Rev. B* **79**, 125443 (2009).
- [55] M. Serbyn and D. A. Abanin, New Dirac points and multiple Landau level crossings in biased trilayer graphene, *Phys. Rev. B* **87**, 115422 (2013).
- [56] K. W. Lee, C. E. Lee, Density functional theory calculations of the electric-field-induced Dirac cones and quantum valley Hall state in ABA-stacked trilayer graphene, *Phys. Rev. B* **92**, 245416 (2015).
- [57] N. J. Zhang, J. X. Lin, D. V. Chichinadze, Y. Wang, K. Watanabe, T. Taniguchi, L. Fu, and J. I. A. Li, Angle-resolved transport non-reciprocity and spontaneous symmetry breaking in twisted trilayer graphene, *Nat. Mater.* **23**, 356 (2024).
- [58] D. Guerci, Y. Mao, and C. Mora, Chern mosaic and ideal flat bands in equal-twist trilayer graphene, [arXiv:2305.03702](https://arxiv.org/abs/2305.03702).
- [59] L. Q. Xia, S. C. de la Barrera, A. Uri, A. Sharpe, Y. H. Kwan, Z. Zhu, K. Watanabe, T. Taniguchi, D. Goldhaber-Gordon, L. Fu, T. Devakul, and P. Jarillo-Herrero, Helical trilayer graphene: a moiré platform for strongly-interacting topological bands, [arXiv:2310.12204](https://arxiv.org/abs/2310.12204).
- [60] T. Devakul, P. J. Ledwith, L. Q. Xia, A. Uri, S. C. de la Barrera, P. Jarillo-Herrero, and L. Fu, Magic-angle helical trilayer graphene, *Sci. Adv.* **9**, eadi6063 (2023).
- [61] C. Zhang, T. Zhu, S. Kahn, T. Soejima, K. Watanabe, T. Taniguchi, A. Zettl, F. Wang, M. P. Zaletel, and M. F. Crommie, Manipulation of chiral interface states in a moiré quantum anomalous Hall insulator, *Nat. Phys.* **20**, 951 (2024).
- [62] N. Nakatsuji, T. Kawakami, and M. Koshino, Multiscale lattice relaxation in general twisted trilayer graphenes, *Phys. Rev. X* **13**, 041007 (2023).
- [63] P. Jiang, X. Tao, H. Hao, Y. Liu, X. Zheng, and Z. Zeng, Two-dimensional centrosymmetrical antiferromagnets for spin photogalvanic devices, *npj Quantum Inf.* **7**, 21 (2021).
- [64] J. An, S. You, Z. Qiao *et al.* (unpublished).
- [65] N. Leconte, S. Javvaji, J. An, A. Samudrala, and J. Jung, Relaxation effects in twisted bilayer graphene: A multiscale approach, *Phys. Rev. B* **106**, 115410 (2022).
- [66] K. Hermann, Periodic overlayers and moiré patterns: theoretical studies of geometric properties, *J. Phys.: Condens. Matter* **24**, 314210 (2012).
- [67] S. Plimpton, Fast parallel algorithms for short-range molecular dynamics, *J. Comput. Phys.* **117**, 1 (1995).
- [68] A. P. Thompson, H. M. Aktulga, R. Berger, D. S. Bolintineanu, W. M. Brown, P. S. Crozier, P. J. in't Veld, A. Kohlmeyer, S. G. Moore, T. D. Nguyen, R. Shan, M. J. Stevens, J. Tranchida, C. R. Trott, and S. J. Plimpton, LAMMPS - A flexible simulation tool for particle-based materials modeling at the atomic, meso, and continuum scales, *Comput. Phys. Commun.* **271**, 108171 (2022).
- [69] M. Wen, S. Carr, S. Fang, E. Kaxiras, and E. B. Tadmor, Dihedral-angle-corrected registry-dependent interlayer potential for multilayer graphene structures, *Phys. Rev. B* **98**, 235404 (2018).
- [70] N. Leconte, J. Jung, S. Lebègue, and T. Gould, Moiré-pattern interlayer potentials in van der Waals materials in the random-phase approximation, *Phys. Rev. B* **96**, 195431 (2017).
- [71] A. N. Kolmogorov and V. H. Crespi, Registry-dependent interlayer potential for graphitic systems, *Phys. Rev. B* **71**, 235415 (2005).
- [72] D. W. Brenner, O. A. Shenderova, J. A. Harrison, S. J. Stuart, B. Ni, and S. B. Sinnott, A second-generation reactive empirical bond order (REBO) potential energy expression for hydrocarbons, *J. Phys.: Condens. Matter* **14**, 783 (2002).
- [73] G. Trambly de Laissardière, D. Mayou, and L. Magaud, Numerical studies of confined states in rotated bilayers of graphene, *Phys. Rev. B* **86**, 125413 (2012).
- [74] N. N. T. Nam and M. Koshino, Lattice relaxation and energy band modulation in twisted bilayer graphene, *Phys. Rev. B* **96**, 075311 (2017).
- [75] P. Moon and M. Koshino, Electronic properties of graphene/hexagonal-boron-nitride moiré superlattice, *Phys. Rev. B* **90**, 155406 (2014).
- [76] R. Yu, X. L. Qi, A. Bernevig, Z. Fang, and X. Dai, Equivalent expression of \mathbb{Z}_2 topological invariant for band insulators using the non-Abelian Berry connection, *Phys. Rev. B* **84**, 075119 (2011).